Available online at www.sciencedirect.com
SCIENCE DIRECT
Polymer 47 (2006) 2984–2996
polymer
www.elsevier.com/locate/polymer

Phenolic resin–trisilanolphenyl polyhedral oligomeric silsesquioxane (POSS) hybrid nanocomposites: Structure and properties

Yudong Zhang [a], Sangho Lee [a], Mitra Yoonessi [c], Kaiwen Liang [b], Charles U. Pittman [a,*]

[a] Department of Chemistry, Mississippi State University, P.O. Box 9573, Mississippi State, MS 39762, USA
[b] Dave C. Swalm School of Chemical Engineering, Mississippi State University, Mississippi State, MS 39762, USA
[c] Air Force Research Laboratory, 2941 P Street, Bldg. 654, Wright-Patterson AFB, OH 45433, USA

Received 12 December 2005; received in revised form 28 February 2006; accepted 1 March 2006

Abstract

The structure and properties of organic–inorganic hybrid nanocomposites prepared from a resole phenolic resin and a POSS mixture containing >95 wt% trisilanolphenyl POSS was investigated by POM (polarized optical microscopy), SEM, TEM, WAXD, FT-IR, DSC, and TGA techniques. Composites with 1.0–10.4 wt% of POSS were prepared by dissolving the POSS and the phenolic resin into THF, followed by solvent removal and curing. Both nano- and micro-sized POSS filler aggregates and particles were shown to be heterogeneously dispersed in the cured matrix by POM, TEM, SEM, and X-EDS. POSS was found everywhere, including in both dispersed phase domains and in the matrix. The nanocomposite morphology appears to form by a multi-step POSS aggregation during the process of phase separation. Both the matrix and dispersed 'particulate' phase domains are mixtures of phenolic resin and POSS. POSS micro-crystals act as the core of the dispersed phase. The bigger dispersed domains consist of smaller particles or aggregates of POSS molecules that exhibit some order but regions of matrix resin are interspersed. A WAXD peak at $2\theta \sim 7.3°$ indicates crystalline order in the POSS aggregates. This characteristic peak's intensity increases with an increase in POSS loading, suggesting that more POSS molecules have aggregated or crystallized. FT-IR spectra confirm that hydrogen bonding exists between the phenolic resin and POSS Si–OH groups. This increases their mutual compatibility, but H-bonding does not prevent POSS aggregation and phase separation during curing. TGA measurements in air confirmed the temperature for 5% mass loss in increases with increase of POSS loading and at $T > 550°$ the thermal stability increases more sharply with POSS loading. The nanocomposite glass transition temperatures (T_g) are only slightly be affected by the POSS filler.

Keywords: Polyhedral oligomeric silsesquioxanes (POSS); Organic–inorganic hybrids nanocomposites; Structure and properties

1. Introduction

The properties of organic–inorganic hybrid nanocomposites depend on the uniform dispersion of fillers, where at least one-dimension less than 100 nm in the polymers matrix. Morphology and structure are important factors governing the properties of nanocomposites. Polyhedral oligomeric silsesquioxanes (POSS) are attracting increased attention in nanostructured organic–inorganic hybrid materials [1–4]. POSS-containing epoxy [5–11], PMMA [12–15], polyolefin [16–19], vinyl ester [20–22], styrene [20–22], dicyclopentadiene (DCPD) [23], cyanate ester [24], and phenolic [25] nanocomposites have been reported. POSS compounds have $(SiO_{1.5})_n$ core cage structures where $n = 8$, 10, or 12 with sizes from 1 to 3-nm in diameter. Organic substituents attached to each cage Si atom can improve compatibility with the polymer matrix. Nevertheless, aggregation and phase separation of POSS into tiny domains commonly occurs [1–25].

Polymerizable substituents on the cages allow the formation of copolymers where POSS becomes part of the polymer chemical structure [4]. Reactive functional groups can also bond POSS to resin molecules, which subsequently cure into thermoset matrixes [3]. However, in both of these situations, tiny POSS domains often form as POSS undergoes self-aggregation in competition with both chemical bonding to, and molecular dispersion in, the matrix. Pure molecular dispersion has been observed in some thermoset matrices [5,24], but such examples to date are still rare. POSS molecules seem to prefer to aggregate or crystallize to form particles, which can reach micron-sizes [5–25].

Morphology and phase separation play a major role in the properties of nanocomposites [18,20,26]. Although individual POSS molecules are, themselves, nanometer-sized fillers,

* Corresponding author. Tel.: +1 662 325 7616; fax: +1 662 325 7611.
E-mail address: cpittman@chemistry.msstate.edu (C.U. Pittman).

0032-3861/$ - see front matter © 2006 Elsevier Ltd. All rights reserved.
doi:10.1016/j.polymer.2006.03.005

materials with molecular POSS dispersion are expected to have different properties than those containing nanometer-sized aggregates or micron-sized particles. Coughlin et al. prepared nanocomposites by incorporating pendant POSS substituents into polyethylene (PE) [18,19]. These nanocomposites had separate populations of crystalline PE and crystalline POSS domains when the polymer was precipitated from solution or solidified from the molten state. The size and amounts of these domains depended upon how the polymer was precipitated or solidified. In the macroscopic molten state, disordered domains of POSS in an environment of molten PE form nanoscaffolds for subsequent PE crystallization on cooling. Alternatively, precipitation from xylene caused the PE component to crystallize, forming a nanoscaffold for later aggregation/crystallization of POSS. Thus, the nano-structure was forced to develop around a preexisting nanoscale scaffold that was formed by domains of a selected component (either PE or POSS). However, the molecular connectivity between the POSS and PE provided a constraint and frustration for crystallization. Indeed, crystallization of either POSS or PE can be significantly suppressed [19].

Nie et al. [11] argued that a kinetic competition between POSS phase separation and cross-linking, during the curing of a non-crystalline epoxy resin, controlled the final morphology and microstructure of epoxy–POSS nanocomposites. When rate of phase separation was faster than that of chemical cross-linking, a macro-heterogeneous morphology was obtained. By catalytically enhancing the cure rate, POSS aggregation could not occur fast enough to give macrophase separation. However, the microstructure was heterogeneous with smaller POSS domains present. No experiment demonstrated that crystalline order was present in this nanocomposite, because the dispersed phase domain sizes were in nanometer range. However, little or no POSS existed as single dispersed molecules.

Matějka [7,8] et al. investigated phase separation in epoxy networks and came to a similar conclusion. Copolymerization of POSS monomers with the epoxy resin generated three series of samples, in which the POSS molecules were (1) bonded pendant onto network chain segments, (2) formed junctions in the network, or (3) were not bonded to the network. The organic–inorganic network structures, morphologies and mechanical properties were mainly governed by POSS–POSS interactions within the organic matrix. The aggregation propensity in the matrix is controlled by the nature of the POSS substituents and by the topological location of POSS moieties. Good resin compatibility assists POSS dispersion. Substituents can affect the incorporated POSS crystal structure. Aggregation or crystallization is promoted by poor compatibility. However, Matějka did not establish how much POSS was grafted to the epoxy network versus the amount which is present as isolated unbonded monomers.

In this study, we investigated the morphology, structure and properties of resole phenolic resin/trisilanolphenyl-POSS nanocomposites using POM, SEM, TEM, WAXD, FT-IR, DSC, and TGA techniques. First, nanocomopsite samples of varying resin/POSS ratios were prepared by co-dissolving this >95 wt% trisilanolphenyl–POSS mixture and the uncured phenolic resin into THF. This was followed by solvent removal and curing. During curing, it is possible that Si–OH groups of the POSS could react with methylol functions of the resole to chemically attach some POSS into the resin network. However, POSS phase separation could occur to varying degrees both during the THF removal and during curing when the entropy of mixing would decrease. A kinetics race can occur among (1) POSS aggregation into domains and (2) POSS chemical bonding into the resin and (3) POSS physical entrapment in the cross-linked matrix as phase separation in slowed by the increasing viscosity and gelation. Finally, TGA and DSC were employed to investigate the thermal stability and glass transition temperature of nanocomposites.

2. Experimental

2.1. Materials

A POSS mixture, PM1271 obtained from Hybrid Plastics Company [1], was used in the form of a white powder. This product was formed during the synthesis of trisilanolphenyl POSS, but it was not further purified. Its major ingredient (more than 95 wt%) is trisilanophenyl-POSS ($C_{42}H_{38}O_{12}Si_7$, molecular weight =931.34 g/mol), which contains a partial T_8 cage with one corner Si missing, leaving three Si–OH functions (Fig. 1). This mixture is less expensive to produce than pure trisilanophenyl–POSS due to its higher yield based on the starting materials employed and due to the reduced number of purification steps required. Nanocomposite stochiometries are given in wt/wt ratios. The resole-type phenolic resin, Hitco 134 A, was purchased from Ashland Company. This resin is composed of phenolic oligomeric components 63.0–67.0 wt%; isopropanol 13.0–17.0 wt%; phenol 10.0 wt%; bis-(2-hydroxyethyl)amine alcohol 3.0–7.0 wt%; water 2.0–6.0 wt% and formaldehyde 1.1 wt%.

2.2. Preparation of samples

Phenolic resin–POSS composites were prepared by weighing phenolic resin samples, removal of isopropanol and water at 70–100 °C (300–350 mmHg) and dissolution of the sample into THF to form transparent homogenous solutions. Then pre-weighed amounts of the POSS mixture,

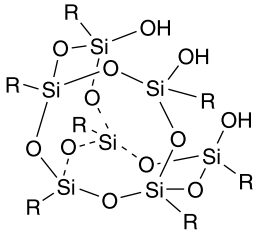

Fig. 1. Trisilanolphenyl–polyhedral oligomeric silsesquioxane (POSS), $C_{42}H_{38}O_{12}Si_7$, MW: 931.34 g/mol.

dissolved in THF, was added into the phenolic resin THF solutions at room temperature to give transparent solutions (2 g/10 ml THF). These solutions were poured into trays made of non-stick paper. THF was removed at 1 atm at ambient temperature for 12 h, followed by heating to 80 °C (300–350 mmHg) for 3 h to remove any residual solvent. The resulting nanocomposite samples were cured at 150 °C for 10 h. Nanocomposites containing 1, 3, 5, 7, and 10.4 wt% of POSS in the resin were prepared along with a reference sample of the pure resin.

2.3. Characterization

2.3.1. Polarized optical microscopy (POM)

A polarizing optical microscope (Olympus) was employed to study phase separation of nanocomposites. A solution (1 g/100 ml) of POSS in the phenolic resin (10 wt%) was dropped onto a glass slide to observe its morphology. After the THF evaporated for 10 min at room temperature, the phase separation process was recorded. Then a drop of THF was added to the slide and the sample was reexamined. Next, the sample was dried in air. A portion of the sample was cured at 150 °C in a vacuum oven (300–350 mmHg) for 5 h. All of the samples were examined under a polarized optical microscope at magnifications of 400 at room temperature (see Fig. 2).

2.3.2. Scanning electron microscopy (SEM) and X-EDS analysis.

A JSM-6500F (JEOL) field emission scanning electron microscope operating at 10 kV was used to examine the nanocomposites' morphologies. The specimens were submerged in liquid nitrogen for 30 min, and fractured cryogenically. One part of each fractured sample was kept for reference, and the other part was extracted by submersion in THF for 30 min at room temperature, washed several times with THF and distilled water and finally dried in air. All samples, including both extracted and virgin surfaces, were thinly sputter-coated with Pt–Au using a Polaron E5100 sputter coater. The morphologies exhibited particle-like domains imbedded in a continuous matrix phase.

The dispersed phase domains and the matrix regions of the original samples were analyzed using an X-EDS spectrometer (Inca-Sight EDS7558 instrument, OXFORD) to determine their Si, O, and C content. The X-EDS volume coverage (surface area and depth, which respond to irradiation) is larger than the particle domains in most cases. Therefore, this limits the resolution and permits only semiquantitive results in the experiments to determine the POSS content in dispersed phase domains. The THF-extracted surfaces were also analyzed by SEM and X-EDS techniques in order to compare with unetched samples. A variety of magnifications from 500 to 20,000 were employed to examine the morphology (see Figs. 3 and 4).

2.3.3. Transmission electron microscopy (TEM)

Phenolic nanocomposite samples were cut into thin (70–80 nm) sections with an ultramicrotome (Reichert-Jung Ultracut E) using a diamond knife at room temperature. Slices were mounted on Formvar or amorphous-carbon-coated copper TEM grids and examined at 80–100 kV by a JEOL JEM-100CX II transmission electron microscope.

2.3.4. Wide angle X-ray diffraction (WAXD)

The crystalline nature of the as-received POSS and powder samples of the phenolic–POSS nanocomposites were characterized by X-ray diffraction using a Bruker AXS D8 diffractometer employing Ni-filtered Cu Kα radiation at room temperature. The X-ray wavelength was 1.54 Å, and the scattering angle, 2θ, was examined between 0 and 30° with 0.1° step lengths. Bragg's law ($\theta = 2d \sin \theta$) was used to determine the distance between planes in crystalline POSS.

2.3.5. Fourier transform infrared spectroscopy (FTIR)

FTIR spectroscopy measurements were performed with a MIDAC FTIR spectrometer (Model 101280-1) using 128 scans at a resolution of 2.0 cm^{-1}. Each spectrum was recorded from 4000 to 500 cm^{-1} at room temperature. Phenolic nanocomposite samples were ground to a fine powder and incorporated into KBr pellets, thin enough to be within a range where the Beer–Lambert law is obeyed.

2.3.6. Differential scanning calorimetry (DSC)

Thermal analysis was carried out using a Perkin–Elmer DSC-7 differential scanning calorimetry (DSC), after calibration with high purity indium. A sample (5–10 mg) was placed on the DSC cell and then heated at scan rate of 20 °C/min within the range of from −30 to 180 °C. Then, the specimen was quickly cooled to −30 °C after the first scan. The second scan was then performed in the same way. The value of T_g was obtained as the midpoint of the transition point of the heat capacity (C_p) change at a scan rate of 20 °C/min over a temperature range from −30 to 180 °C.

2.3.7. Thermal gravimetric analysis (TGA)

The thermal stabilities of the composites in air were measured using a TA Hi-Resolution TGA 2950 (TA Instruments, Inc., New Castle, DE). Samples (10–15 mg) were loaded in aluminum pans, ramped to 900 °C (10 °C/min). The mass change was recorded with reference to empty aluminum pans. The air flow rate was 25 ml/min.

3. Results and discussion

When POSS and the resole phenolic resin's oligomers were dissolved in THF, a homogenous, transparent light-yellow solution was obtained, without any phase separation. However, as THF evaporated, the solution eventually changed into soft phenolic resin-containing solvent. Its transparency gradually decreased to semi-transparent. The color became dark-brown when all the THF had been removed. After curing at 150 °C, the samples with POSS become more opaque. The transparency decreases progressively with increasing POSS loading.

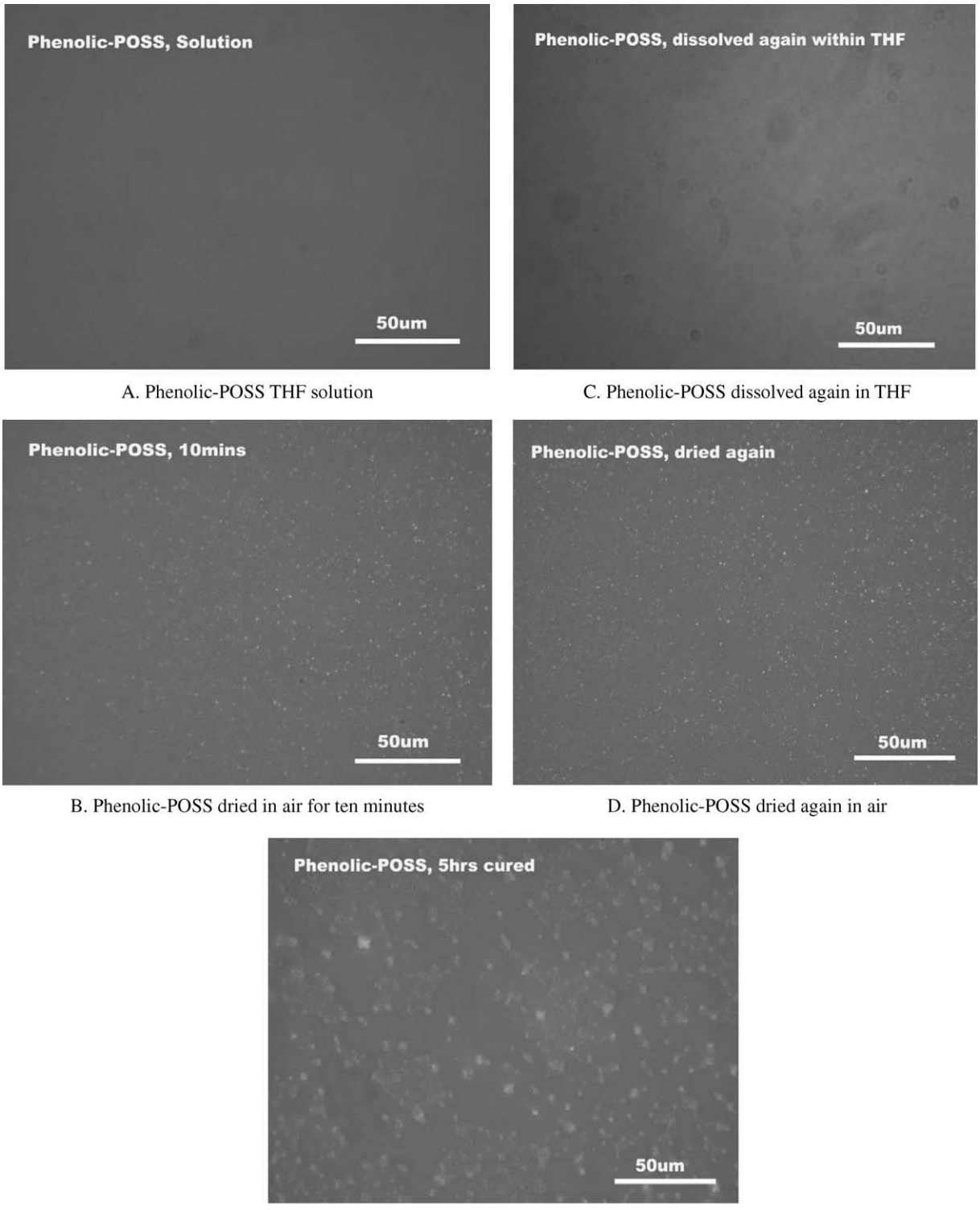

Fig. 2. POM images (magnification 400) of the 10.0 wt% POSS nanocomposites samples. (A) Phenolic–POSS THF solution. (B) Phenolic–POSS dried in air for 10 min. (C) Phenolic–POSS dissolved again in THF. (D) Phenolic–POSS dried again in air. (E) Phenolic–POSS cured for 5 h at 150 °C.

3.1. Optical microscopy

POM images (Fig. 2) confirmed that no phase separation occurs in the phenolic–POSS (9:1 wt/wt) THF solution during most of the THF evaporation (Fig. 2(A)). This was the highest POSS concentration employed in any of the composite syntheses. When THF was removed in air for 10 min, small white dots appeared, indicating that phase separation had

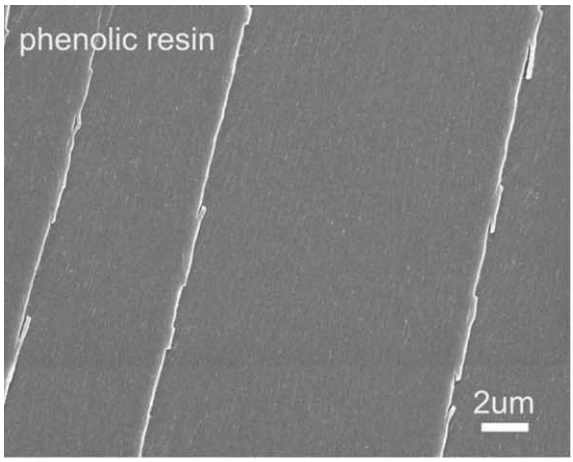

A. Reference phenolic resin (0 wt% POSS).

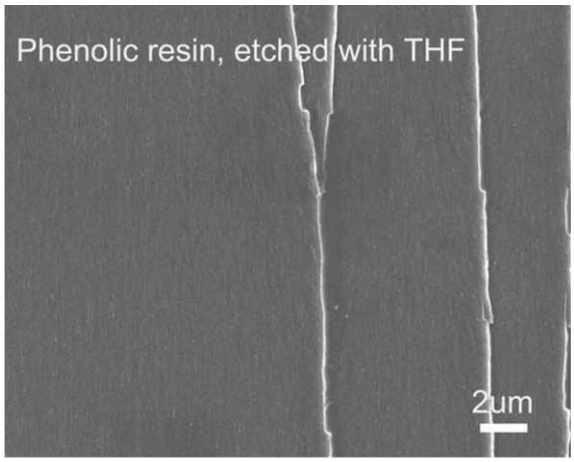

B. Reference phenolic resin (0 wt% POSS) after THF surface extraction.

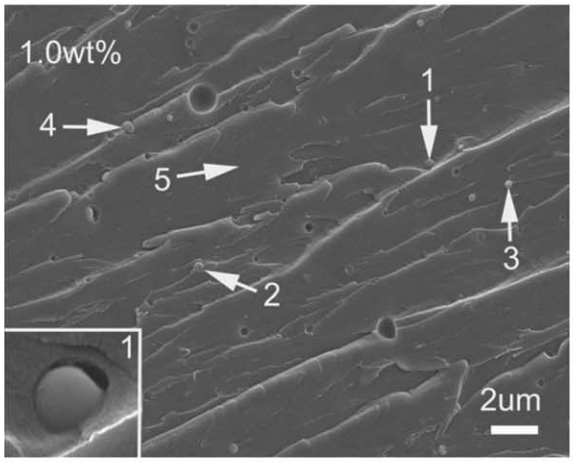

C. Phenolic resin/1.0 wt% POSS (numbers show EDX analysis location).

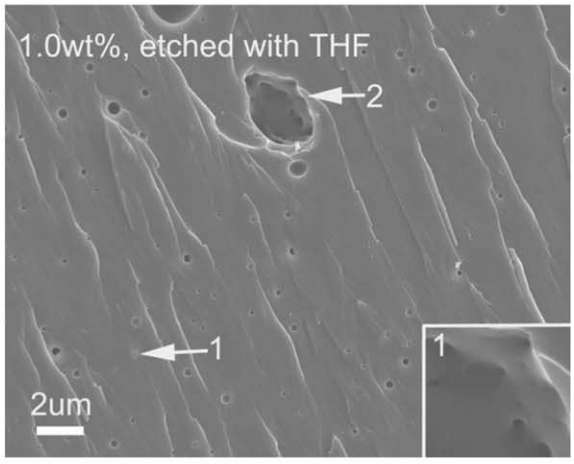

D. Phenolic resin/1.0 wt% POSS after THF surface extraction (numbers show EDX analysis locations).

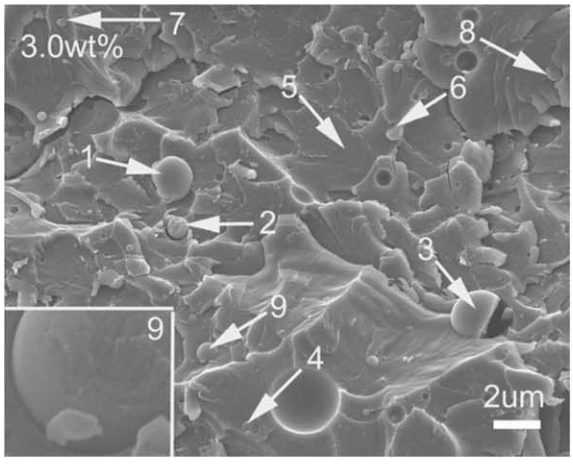

E. Phenolic resin/3.0 wt% POSS (numbers show EDX analysis locations).

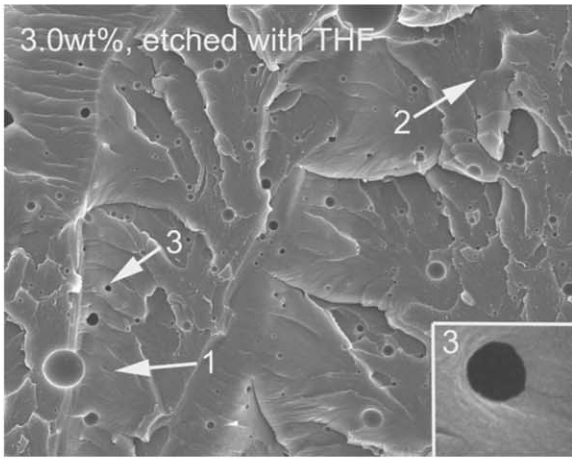

F. phenolic resin/3.0 wt% POSS after THF surface extraction (numbers show EDX analysis locations).

Fig. 3. SEM images (5 K) of phenolics POSS nanocomposites with 0, 1.0, 3.0, 5.0, 7.0, and 10.4 wt% POSS with higher magnification inset images in micrographs C–L. (A) Reference phenolic resin (0 wt% POSS). (B) Reference phenolic resin (0 wt% POSS) after THF surface extraction. (C) Phenolic resin/1.0 wt% POSS (numbers show EDX analysis location). (D) Phenolic resin/1.0 wt% POSS after THF surface extraction (numbers show EDX analysis locations). (E) Phenolic resin/3.0 wt% POSS (numbers show EDX analysis locations). (F) phenolic resin/3.0 wt% POSS after THF surface extraction (numbers show EDX analysis locations). (G) Phenolic resin/5.0 wt% POSS (numbers show EDX analysis locations). (H) Phenolic resin/5.0 wt% POSS after THF surface extraction (numbers show EDX analysis locations). (I) Phenolic resin/7.0 wt% POSS (numbers show EDX analysis locations). (J) Phenolic resin/7.0 wt% POSS after THF surface extraction (numbers show EDX analysis locations). (K) Phenolic resin/10.4 wt% POSS (numbers show EDX analysis locations). (L) Phenolic resin/10.4 wt% POSS after THF surface extraction (numbers show EDX analysis locations).

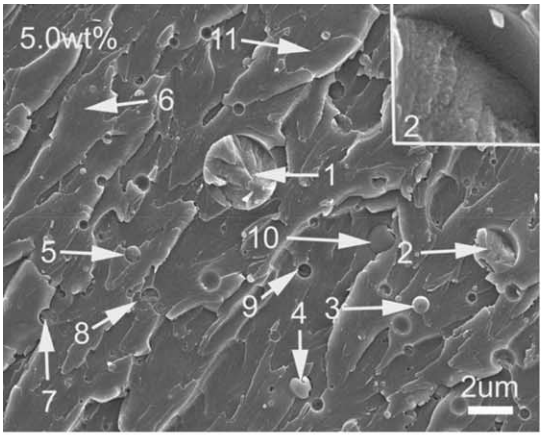

G. Phenolic resin/5.0 wt% POSS
(numbers show EDX analysis locations).

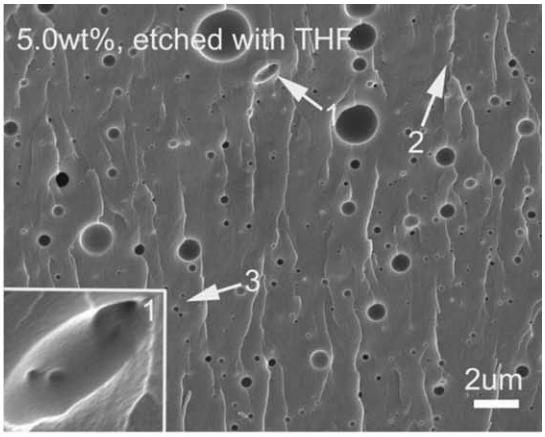

H. Phenolic resin/5.0 wt% POSS after THF surface
extraction (numbers show EDX analysis locations).

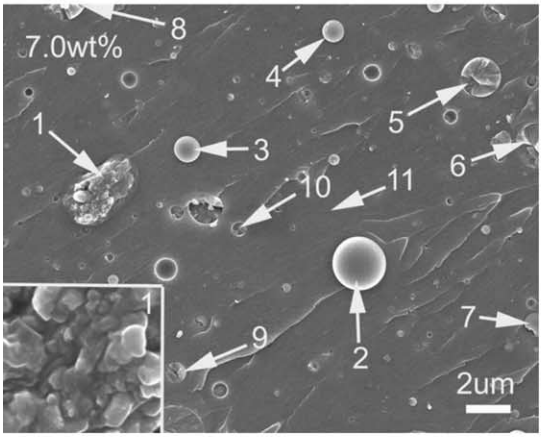

I. Phenolic resin/7.0 wt% POSS
(numbers show EDX analysis locations).

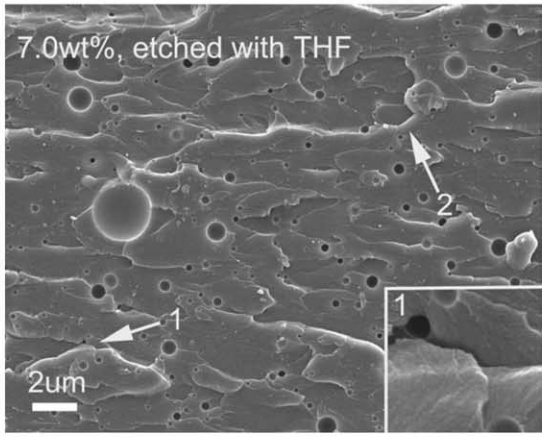

J. Phenolic resin/7.0 wt% POSS after THF surface
extraction (numbers show EDX analysis locations).

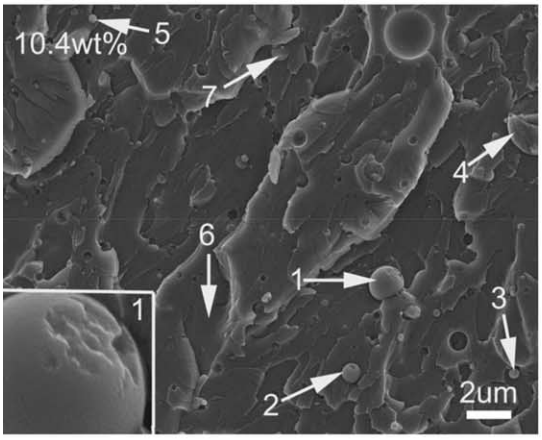

K. Phenolic resin/10.4 wt% POSS
(numbers show EDX analysis locationss).

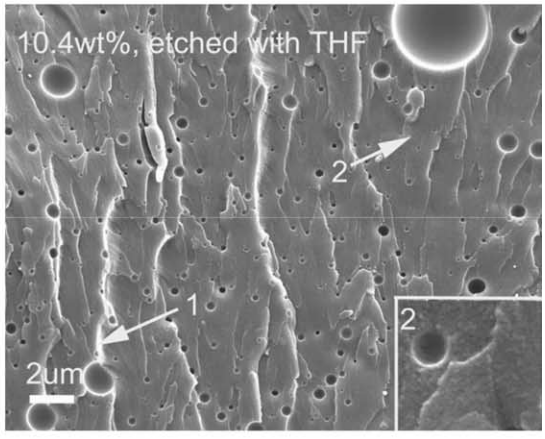

L. Phenolic resin/10.4 wt% POSS after THF surface extraction
(numbers show EDX analysis locations).

Fig. 3 (*continued*)

started. POSS domain formation occurs when most of the THF has been removed (Fig. 2(B)). When this film was again exposed to a drop of THF, all of the white dots immediately disappeared. However, regions of high POSS concentration dissolved in the THF can be observed as THF diffused throughout the film (Fig. 2(C)). The white phase-separated regions reappear after the samples were dried once again (Fig. 2(D)).

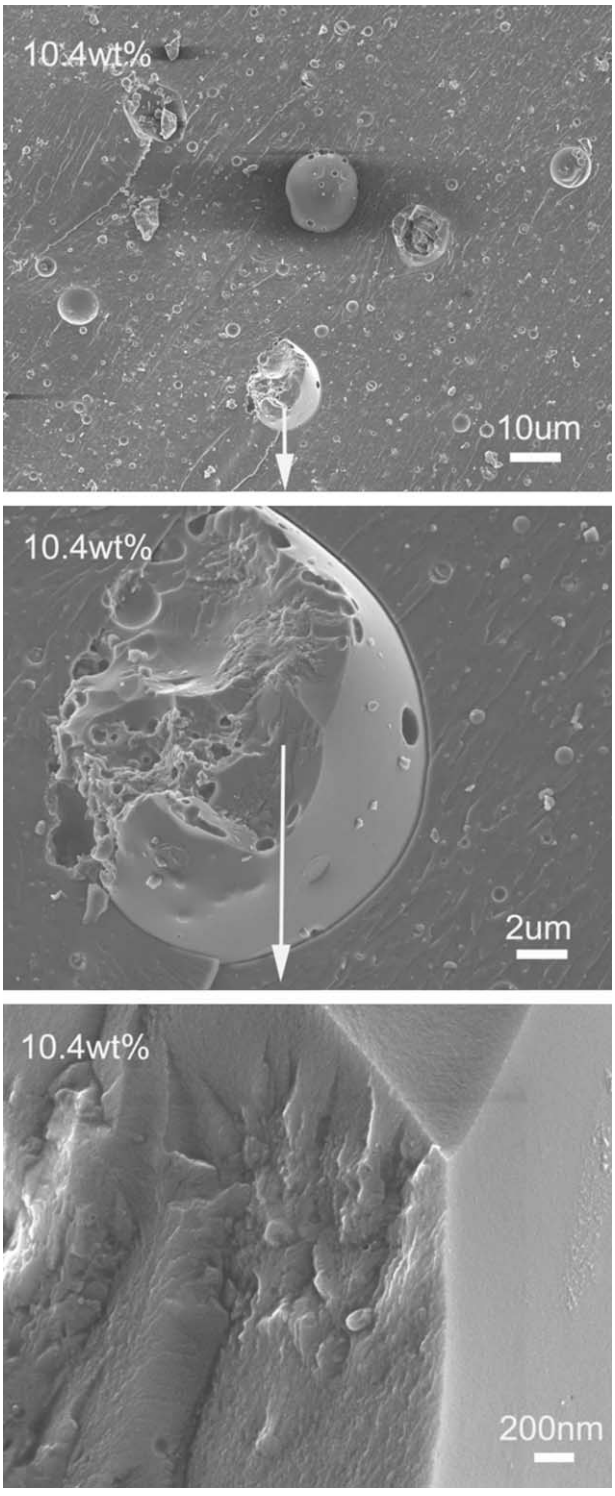

Fig. 4. SEM images of the 10.4 wt% POSS samples with a variety of magnification.

After curing this 10 wt% POSS/resin for 5 h at 150 °C, the phase-separated POSS regions have become larger and appear more diffuse (Fig. 2(E)). This is in agreement with the decreased transparency after curing. The POSS molecules start aggregating and form crystals during the final stages of solvent removal. Curing then enhances phase separation. According to a previous study [27], the crystalline form of POSS does not change during curing. However, crystal defects may increase because of interactions between the phenolic resin and POSS in microcrystals. In WAXD analyses, we have found some POSS peaks broaden.

3.2. SEM analyses

Fig. 3 displays a group of SEM images of the samples with 0, 1.0, 3.0, 5.0, 7.0, and 10.4 wt% POSS, showing the relationship between diameter and the number density of dispersed phase particles and the POSS loading. Each of these micrographs demonstrates large numbers of much smaller (nanometer-sized) domains are present along with that larger micron-sized domains. A comparison between the virgin and the THF-extracted surfaces was made. Clearly, both surface-extracted and virgin surfaces of the sample without POSS are smooth. Neither particles nor holes appear. However, the image of the non-etched samples with 1.0, 3.0, 5.0, 7.0, and 10.4 wt% POSS display numerous micron-sized particles on their fracture surfaces. The number of particles increases as POSS loading increases. After THF extraction, holes appear where POSS aggregates had been and the hole sizes matched the size distribution of the original particulate domains. The dissolution of these POSS regions shows that chemical bonding between methylol and silanol functions did not occur in these regions.

Specific sites were chosen in the SEM micrographs (Fig. 3) and examined at higher magnifications. Inset pictures of higher magnification are given in the corners of these SEM micrographs. These insets indicate a complicated morphology. For example, site 2 in micrograph G (5.0 wt% POSS sample) and site 1 in micrograph K (10.4 wt% POSS sample) show the morphologies. Site 2 in G is particularly instructive. Very small spherical bodies are packed and bonded together within the larger particle. Site 2 in micrograph D (1.0 wt% POSS) and the site 1 in micrograph H (5.0 wt% POSS) further illustrate this morphology.

Fig. 4 provides a set of SEM images of the 10.4 wt% POSS sample at magnifications, which increase from top to bottom. A portion of the top image (magnification 500) was enlarged in the middle image to 2500. Also one site in the middle image was further expanded to 2×10^4 in the bottom image. These images illustrate the complicated morphology at the micro-structure level, which forms in the matrix resin during domain development. The dispersed phase domains often contain both smaller particles and matrix. This suggests the initial nucleation of small particles occurs followed by further aggregation of these small regions.

The THF surface-extracted fracture samples display numerous holes with a variety of diameter sizes. These holes are due to removal of the dispersed phase domains by THF leaching (Fig. 4(D), (F), (H), and (J)). The distribution of hole diameters was determined for hole sizes above 70 nm. Particles or holes with smaller diameters than this could not be accurately seen or measured. These distributions are

shown as histograms in Fig. 5. A wide distribution of hole diameter sizes is observed. Most have diameters less than 800 nm and a large number are below 100 nm in diameter. The number density of the domains increases and their morphological structure become more complicated with an increase of POSS loading. Nevertheless, the mean diameter does not appear to increase with larger amounts of POSS incorporation. However, the number of larger domains

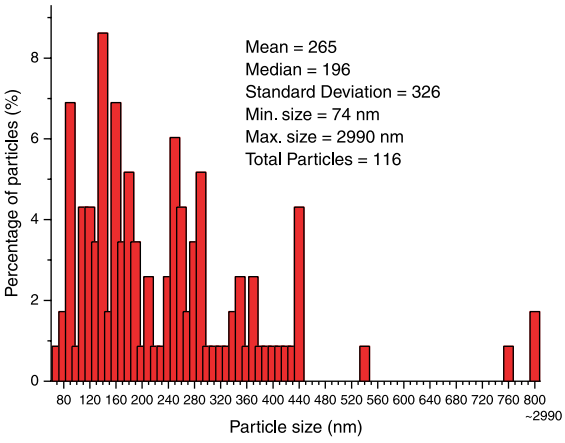

A. Phenolic resin/1.0 wt% POSS after THF surface extraction.

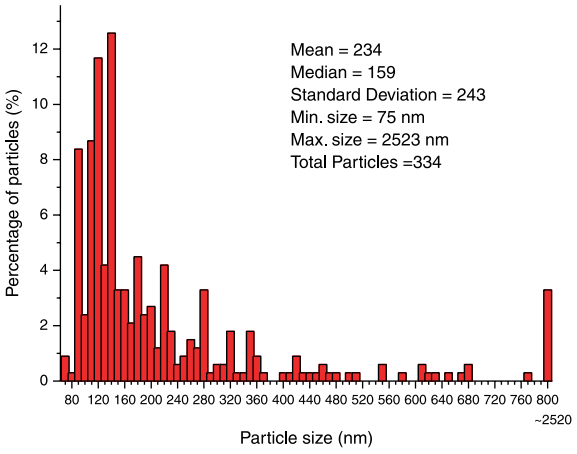

C. Phenolic resin/5.0 wt% POSS after THF surface extraction.

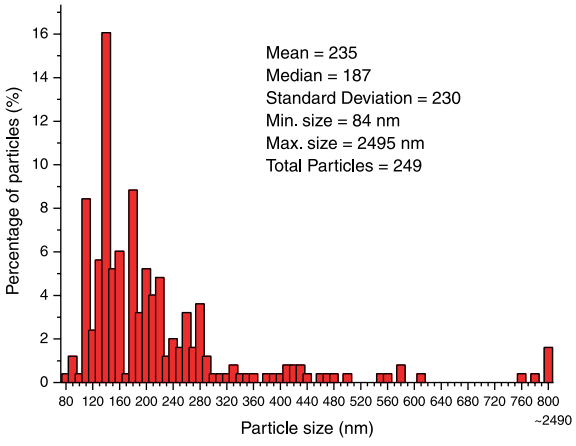

B. Phenolic resin/3.0 wt% POSS after THF surface extraction.

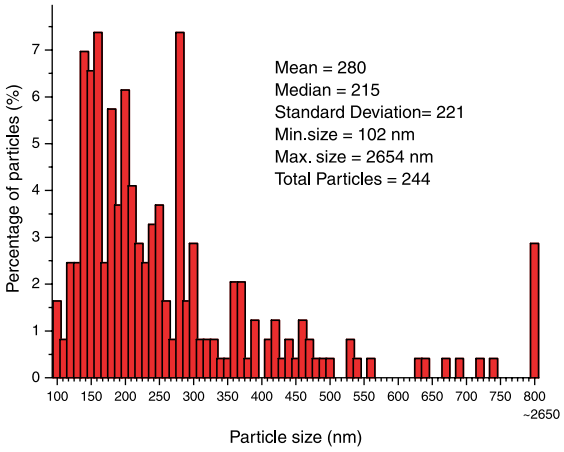

D. Phenolic resin/7.0 wt% POSS after THF surface extraction.

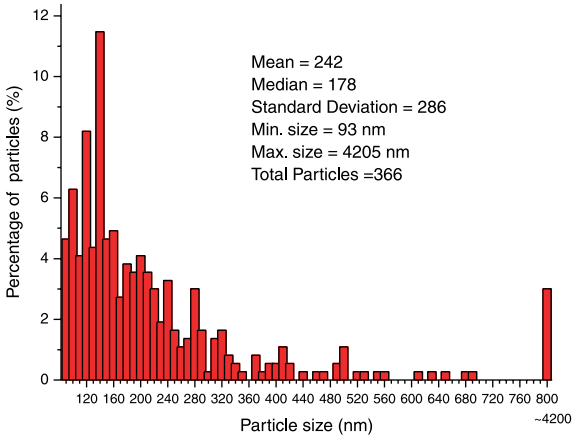

E. Phenolic resin/10.4 wt% POSS after THF surface extraction.

Fig. 5. The domain diameter distribution of the samples. (A) Phenolic resin/1.0 wt% POSS after THF surface extraction. (B) Phenolic resin/3.0 wt% POSS after THF surface extraction. (C) Phenolic resin/5.0 wt% POSS after THF surface extraction. (D) Phenolic resin/7.0 wt% POSS after THF surface extraction. (E) Phenolic resin/10.4 wt% POSS after THF surface extraction.

(diameters >800 nm) increases with larger POSS loadings. The larger domains often consist of smaller aggregated finer domain structures.

3.3. X-EDS analyses

X-EDS analysis was employed to study the dispersed phase domains and the matrix. The spacial resolution of the X-EDS technique is limited due to X-ray scattering with its pronounced tendency to decay, moving outward from the point where the beam impinges. Resolution also depends on the spot size. Thus, X-EDS elemental analyses of particles in a nanometer-size region cannot be accurately measured. Particles in the micron size range give more accurate values.

It was immediately clear that no Si was found in any of the THF-extracted surfaces. This indicates that all the POSS had been completely removed from the fractured surfaces by THF extraction. Thus, any aggregates, particles or molecularly dispersed POSS has been dissolved and removed from depths deeper than X-EDS has an ability to probe. The absence of Si in these analyses suggests very little POSS could have been chemically bonded into the phenolic resin matrix during curing. Physically dispersed POSS greatly predominates in these composites.

In contrast, X-EDS of the unextracted composite samples exhibited Si everywhere. POSS can easily be detected both in dispersed phase domains and in matrix regions where no particles are observed. This was true for the 1.0, 3.0, 5.0, 7.0, and 10.4 wt% POSS samples. The amount of POSS (from silicon analyses) found at specific locations in these composites is summarized in Table 1. The particle diameter is also given at each of these locations except where the beam was impinged only on the matrix (this is indicated by an M in Table 1). X-EDS analyses confirmed that dispersed phase particles contain both POSS molecules and phenolic resin. This was found even for the largest (micron-sized) dispersed domains where the X-EDS-determined elemental contributions from neighboring matrix region would be much smaller than those determined when analyzing a smaller particle. This feature was found at all POSS loadings.

Significant amounts of resin must be present in these dispersed (particulate) domains based on their much lower weight percentage Si contents compared to that of pure POSS. These dispersed phase domains are not primarily crystalline solid POSS particles or aggregates of only POSS molecules as described previously for epoxy–phenyltrisilanol POSS nanocomposites [11]. Instead, these domains are a mixture containing finer quasi-crystalline POSS particles of various sizes plus some phenolic resin.

POSS molecules are also found in regions of the matrix. In principle, the POSS content in the matrix should be far lower than that in dispersed phase domains. However, the POSS content in some dispersed particulate domain regions was actually lower than that found in some regions that appear to be only matrix. The 7.0 wt% POSS composite, for example, had a site in the matrix region with 13.8 wt% POSS. This POSS weight percentage was higher than all other sites sampled on that composite, including sites where the beam was impinged directly on dispersed phase particles.

As POSS loading increases, the content of the POSS found in the matrix region displays a general tendency to increase. This was determined by analyzing the silicon percent at a large number of sites that appear to be only matrix and then averaging them. Some representative data is given in Table 1. A large range of specific POSS weight percents were found within different matrix regions of the same sample in all cases, requiring that averages be taken over many locations. Clearly, the POSS content is quite variable (on the X-EDS sampling scale) throughout all the samples. For example, the POSS content in some matrix regions and in some particles can be higher in samples with 1.0, 3.0, 5.0 wt% POSS than in some corresponding regions of the composites with 7.0, 10.4 wt% POSS. This suggests that the POSS dispersion in the matrix is very complicated, irregular and heterogeneous. It is difficult to establish the exact percentage of POSS within various dispersed phase particle domains, but it appears that

Table 1
The weight percentage of POSS present at both particle and matrix locations in the POSS/phenolic nanocomposites, determined by X-EDS Si elemental analysis

Samples	POSS (wt%) and dispersed phase particles size (μm) at local sites[a]				
	1.0 wt% POSS	3.0 wt% POSS	5.0 wt% POSS	7.0 wt% POSS	10.4 wt% POSS
Analysis site					
1	0 (0.45)	4.8 (1.74)	4.2 (3.29)	5.7 (3.08)	9.8 (1.59)
2	3.1 (0.30)	2.5 (0.93)	4.9 (1.00)	3.4 (2.39)	5.1 (0.84)
3	3.0 (0.32)	5.7 (5.96)	3.1 (0.73)	8.2 (1.20)	5.6 (0.45)
4	8.8 (0.59)	8.7 (0.67)	11.9 (1.01)	9.3 (0.99)	6.4 (1.00)
5	8.6 (M)	3.2 (M)	9.4 (0.67)	5.6 (1.78)	14.3 (0.37)
6		4.8 (0.71)	5.3 (M)	7.0 (1.00)	4.2 (M)
7		4.5 (0.43)	10.1 (0.82)	4.8 (1.12)	3.9 (0.84)
8		2.4 (0.79)	6.9 (0.80)	3.0 (1.91)	
9			4.5 (0.59)	11.5 (0.97)	
10			5.2 (1.29)	5.2 (0.64)	
11			0 (M)	13.8 (M)	

The numbers in parentheses represent the diameter of the particle being examined. The numbers not in parentheses are the wt% of POSS present at each location.
[a] The term (M) represents a site selected in the matrix where no dispersed phase could be imaged.

all dispersed phase domains do not have the same compositions.

3.4. TEM analyses

TEM was employed to study the finer size-scale levels of the internal morphologies. Sections about 75 nm thick contain entire small-sized domains and portions of larger-sized domains. Fig. 6 shows a set of images from samples with 0, 1.0, 5.0, and 10.4 wt% POSS. No dispersed phase domains existed in the pure phenolic resin sample. However, all samples with POSS clearly show numerous dispersed phase domains, each with a wide-size distribution. The particle number density and complexity increases with loading, in agreement with SEM experiments. For example, numerous small particles are found in the TEM image of a dispersed phase domain in the 10.4 wt% POSS sample. The inset images H and I in Fig. 6 are expansions of features seen in TEM micrographs of 5.0 and 10.4 wt% POSS samples, respectively, illustrating this non-homogeniety. Smaller black dots are found in the inset I illustrating that this domain consists of smaller dispersed phase particles plus matrix. A dispersed phase aggregate (white) appears in inset H, suggesting that smaller aggregates of POSS tend to cluster together rather than becoming uniformly dispersed in matrix.

These and other TEM observations support the existence of a complex morphology arising through a series of steps during solvent removal and curing. This process may be similar to the multi-step formation of the complex morphology found in triphenylsilanol POSS–cynante ester nanocomposites [24]

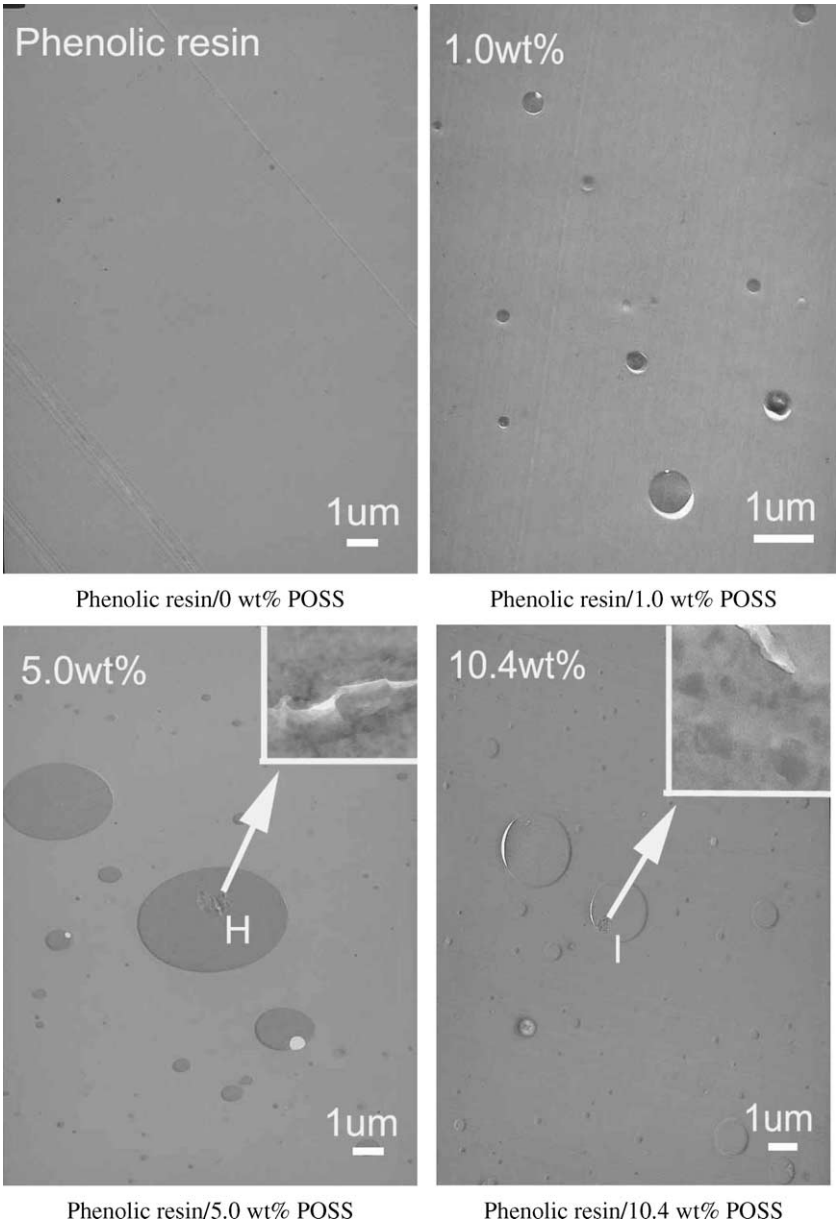

Fig. 6. TEM images of the 0, 1.0, 5.0, 10.4 wt% POSS composite samples.

through evidence provided by small angle neutron scattering (SANS) and TEM. SANS detected POSS aggregates and particles with sizes from 60 to >900 Å. The shape of these phases changed as the size increased. This pattern was consistent with an aggregation mechanism where individual POSS molecules nucleate into tiny aggregates. These initial aggregates then tended to organize into string-like units. As their size increases, these 'strings' thicken and further broaden into disk-like regions. As the size increases further, the POSS domains become more spherical or fractal-like in shape and resin was also included. While no evidence is available for this specific aggregation pattern in the phenolic resin/POSS composites discussed here, domain formation must be a multi-step process.

3.5. WAXD analyses

The WAXD patterns of 1.0, 3.0, 5.0, 7.0, and 10.4 wt% POSS phenolic composites are given in Fig. 7 together with those of the pure POSS powder and the phenolic resin to serve as references. Two major peaks occur. First, a very broad peak appears from $2\theta = 10$–$30°$, corresponding to the amorphous structure peak of the reference phenolic resin. A second peak occurs at $2\theta = 7.3°$, which corresponds to the large peak found for the as-received POSS powder at $2\theta = 7.3°$ (left twin peaks). This peak indicates that POSS can aggregate in the matrix as micro-crystals. The distance (Å) between crystalline planes is around 12.1 Å. Apparently, this characteristic peak in nanocomposite samples is broadened because more defects and less regularity exist in the POSS micro crystals. Such defects may result from interaction between the matrix and the POSS. As POSS loading increases, the intensity of this $2\theta \sim 7.3°$ POSS peak in the composite increases. Furthermore, the highest peak intensity occurs at a scattering angle that increases slightly as the weight percent POSS goes up. As POSS loading increases, more and larger particles exist and these likely would have more highly ordered POSS packing on average. This would lead to a higher fraction of POSS having slight smaller lattice distances.

3.6. FT-IR analyses

FT-IR spectra of the 0, 1.0, 3.0, 5.0, 7.0, and 10.4 wt% POSS composites over the range 2500–3800 cm^{-1}, measured at room temperature, are displayed in Fig. 8. The pure phenolic resin displays two hydroxyl components. A very broad peak for hydrogen-bonded hydroxyl groups is centered at 3356 cm^{-1} [25]. A smaller shoulder at 3505 cm^{-1} corresponds to free hydroxyl groups. As POSS loading increases, this main hydrogen-bonded OH peak initially shifts to progressively higher frequencies: 3375 cm^{-1} (3.0 and 5.0 wt%), but then reverts to a lower wavenumber, 3352 cm^{-1}, (7.0 wt%) and finally to 3347 cm^{-1} (<10.4 wt%), and a significant fraction of all POSS molecules cannot hydrogen-bond to the resin since

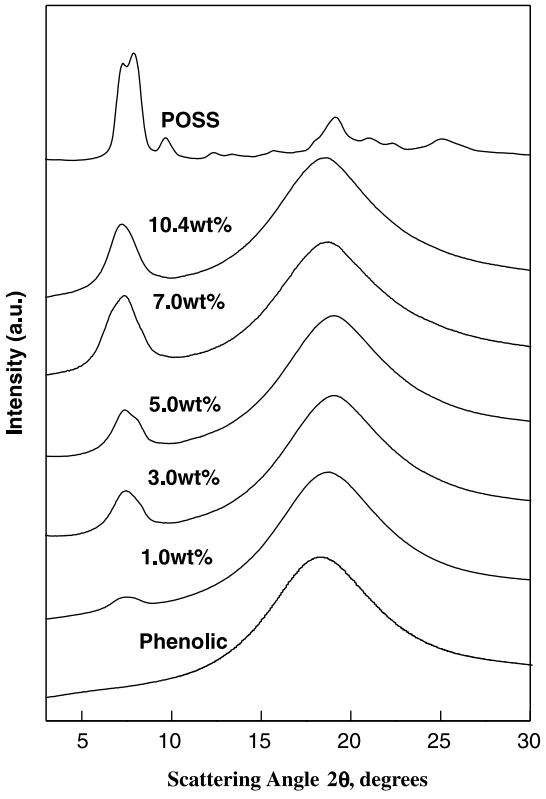

Fig. 7. WAXS curves of the 0, 1.0, 3.0, 5.0, 7.0, 10.4 wt% POSS composite samples and pure POSS.

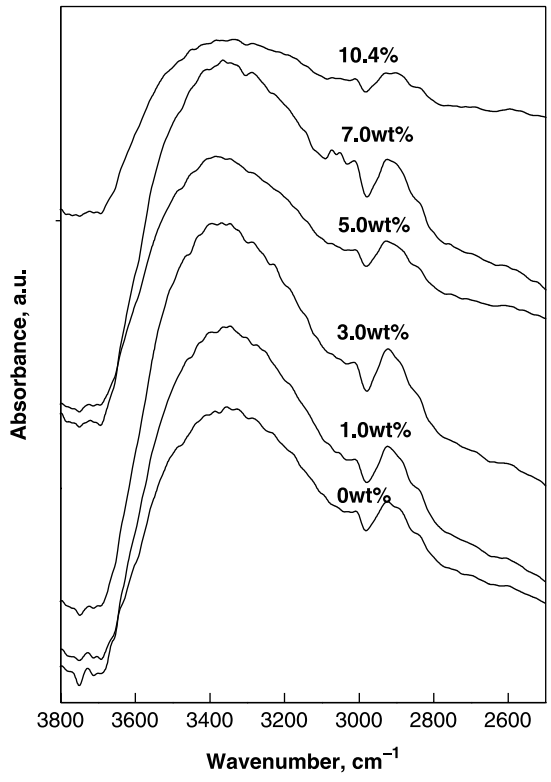

Fig. 8. FT-IR spectra of the 0, 1.0, 3.0, 5.0, 7.0, 10.4 wt% POSS composite samples.

they are inside microcrystals. This behavior is due to POSS/resin compatibility promoted by intermolecular phenolic hydroxyl/silanol hydrogen bonding according to Li et al. [25]. Simultaneously, the intensity of the 3505 cm^{-1} absorption for free hydroxyl groups becomes progressively weaker as the POSS loading increases. This causes the free hydroxyl group content of the resin to decrease as the more acidic POSS hydroxyls hydrogen bond to the phenolic resin. The range of the frequency shifts appears small because POSS loading is low (<10.4 wt%), and a significant fraction of all POSS molecules cannot hydrogen bond to the resin since they are inside microcrystals. In addition, the IR band at 10.4 wt% of POSS loading appears to be more complicated and more broadened, verifying that this sample has more complicated variety of hydrogen bonds as might be expected. This result is consistent with the SEM and TEM analyses of the complex morphology of the 10.4 wt% POSS sample. Table 2 summarizes these data.

POSS–resin hydrogen bonding assists POSS/resin compatibility and aids dispersion. Nevertheless, trisilanolphenyl POSS has only limited solubility in the resin. Upon THF removal, some POSS phase separates from the uncured phenolic resin loaded with 10.4 wt% POSS. Solubility decreases during curing as the entropy of mixing drops and as methylol hydroxyl groups of the resole are consumed. Thus, POSS aggregation progresses as the curing advances. This aggregation is resisted by the viscosity increase and by POSS-to-resin H-bonding. Gelation further restricts this process and finally locks in the existing morphology at that point of the cure. Some POSS is molecularly locked into the matrix along with other very tiny aggregates in the nanometer size range. Small aggregates exist as separate domains. As they further aggregate and cluster together, and resin regions are incorporated into well-defined domains as the domain size increases. The amount of insoluble POSS is greater during every stage of this process at higher POSS loadings but the specific effects of POSS loading on morphology development are not well understood. The morphology and structure affect the properties of phenolic–POSS nanocomposites, particularly the higher temperature thermal properties.

3.7. DSC analyses

Scanning calorimetry was used to measure the glass transition temperature of these nanocomposites. The values of T_g were obtained using compositions with each POSS loading (0, 1.0, 3.0, 5.0, 7.0, and 10.4 wt%). Each composition exhibited a single T_g. The T_g increases from 60 to 62 °C as POSS loading increases from 0 to 10.4 wt%, so POSS has only a very small effect on glass transition temperatures. Only the interfacial POSS units in the micro crystals can H-bond to the phenolic resin. Most of the POSS molecules are inside the aggregates and have no chance of affecting segmental motion in the crosslinked phenolic matrix.

Table 2
FT-IR locations of the main O–H stretching peak and its shoulder peak in the 0, 1.0, 3.0, 5.0, 7.0, and 10.4 wt% POSS samples

Nanocomposite POSS loading (wt%)	0	1.0	3.0	5.0	7.0	10.4
Main peak, (cm^{-1})	3356	3356	3375	3375	3352	3347
Shoulder peak, (cm^{-1})	(3505)	(3505)	–	–	–	–

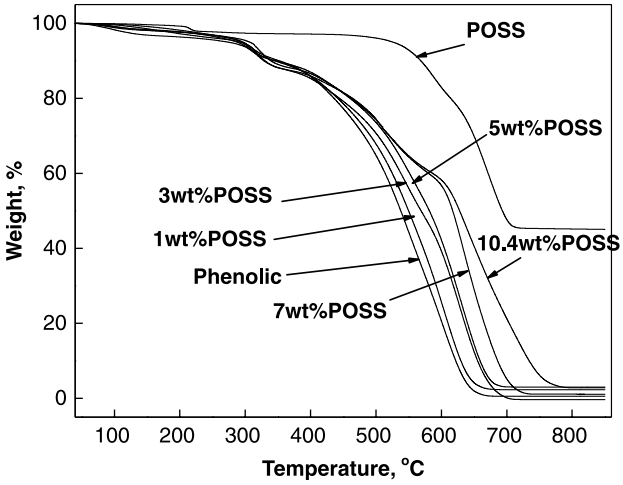

Fig. 9. TGA curves of nanocomposite samples with 0, 1.0, 3.0, 5.0, 7.0, 10.4 wt% POSS and pure POSS.

3.8. TGA analyses

The nanocomposite thermal stabilities were examined in air using TGA at a 10 °C/min heating rate (Fig. 9). The temperature at which a 5 wt% mass loss was reached (T_d5) rose (273, 288, 293, 296, 295, and 307 °C) as the POSS loading increased from 0, 1.0, 3.0, 5.0, 7.0 to 10.4 wt%. The T_d5 of the pure POSS is 526 °C. The temperature at which a 50 wt% mass loss had occurred (T_d50) increases from 537, 549, 569, 581, 617 to 627 °C as the POSS loading increases from 0, 1.0, 3.0, 5.0, 7.0 to 10.4 wt%. The T_d50 of the pure POSS is 693 °C. The presence of trisilanolphenyl POSS markedly increases the thermal air stability of these phenolic composites. The mechanism of this observation is unknown.

4. Conclusions

Phase separation during POSS/phenolic resin nanocomposite formation causes a complex morphology to form. A multistep aggregation phase separation such as that approximated in Scheme 1 generates the observed microstructure. The micron-sized dispersed phase particles contain smaller POSS aggregates/particles together with phenolic resin. A degree of crystallinity exists within the POSS-rich domains but the average degree of order is less then that of highly purified trisilanophenyl POSS. The final composite morphology has not

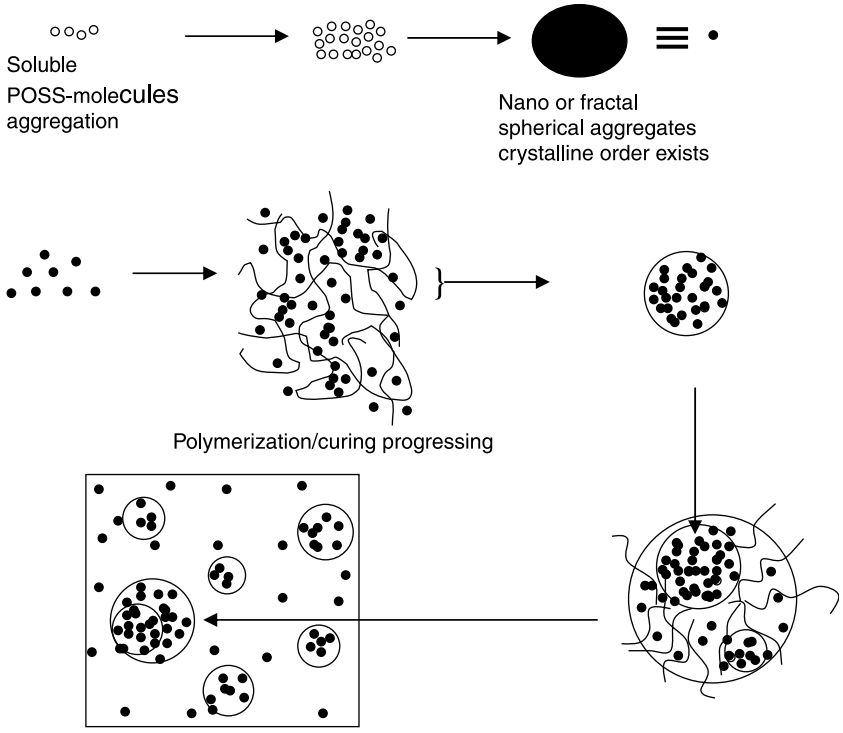

Scheme 1. Formation of POSS nanocomposite morphology during phase separation.

reached thermodynamic equilibrium. Instead, it has been locked into a quasi-equilibrated state.

POSS silanol/phenolic hydroxyl hydrogen bonding increases the compatibility. This is beneficial for POSS dispersion in matrix but cannot prevent phase separation.

The thermal stability as measured by the temperatures at which 5 or 50% wt loss occurs increases with an increase in the POSS loading. The glass transition temperature (T_g) of nanocomposites is only slightly be affected by the loading of POSS.

Acknowledgements

This work was supported in part by the Air Force Office of Scientific Research (Grant no. F 49620-02-1-026-0), STTR (Grant no. FA955005C0028) and the National Science Foundation (Grant no. EPS0132618).

References

[1] POSS is a registered trademark of Hybrid Plastics, www.hybridplastics.com.
[2] Baney RH, Itoh M, Sakakibara A, Suzuki T. Chem Rev 1995;95:1409.
[3] Pittman Jr CU, Li G, Ni H. Macromol Symp 2003;196:301.
[4] Li G, Wang LC, Ni H, Pittman Jr CU. Inorg Organomet Polym 2001;11:123.
[5] Li G, Wang LC, Toghiani H, Daulton TL, Koyama K, Pittman Jr CU. Macromolecules 2001;34:8686.
[6] Maria JB, Luis B, Diana PF, Roberto W. Macromolecules 2003;36:3128.
[7] Matějka L, Strachota A, Pleštil J, Whelan P, Steinhart M, Sÿlouf M. Macromolecules 2004;37:9449.
[8] Strachota A, Kroutilova I, Kovarova J, Matějka L. Macromolecules 2004;37:9457.
[9] Baker ES, Gidden J, Anderson ES, Haddad TS, Bowers MT. Nano Lett 2004;4:779.
[10] Choi J, Kim SG, Laine RM. Macromolecules 2004;37:99.
[11] Liu H, Zheng S, Nie K. Macromolecules 2005;38:5088.
[12] Li G, Cho H, Wang LC, Toghiani H, Pittman Jr CU. J Polym Sci, Part A: Polym Chem 2004;43:355.
[13] Huang QR, Volksen W, Huang E, Toney M, Frank CW, Miller RD. Chem Mater 2002;14:3676.
[14] Anderson SE, Baker ES, Mitchell C, Haddad TS, Bowers MT. Chem Mater 2005;17:2537.
[15] Kopesky ET, Haddad TS, McKinley GH, Cohen RE. Polymer 2005;46:4743.
[16] Fu BX, Yang L, Somani RH, Zong SX, Hsiao BS, Phillips S, et al. J Polym Sci, Part B: Polym Phys 2001;39:2727.
[17] Zheng L, Farris RJ, Coughlin EB. Macromolecules 2001;34:8034.
[18] Zheng L, Waddon AJ, Farris RJ, Coughlin EB. Macromolecules 2002;35:2375.
[19] Waddon AJ, Zheng L, Farris RJ, Coughlin EB. Nano Lett 2002;2:1149.
[20] Romo-Uribe A, Mather PT, Haddad TS, Lichtenhan JD. J Polym Sci, Part B: Polym Phys 1998;36:1857.
[21] Li G, Wang LC, Toghiani H, Pittman Jr CU, Daulton TL. Polymer 2002;43:4167.
[22] Lee A, Xiao J, Feher FJ. Macromolecules 2005;38:438.
[23] Constable GS, Lesser AJ, Coughlin EB. Macromolecules 2004;37:1276.
[24] Liang KW, Li G, Toghiani H, Koo JH, Pittman Jr CU. Chem Mater 2006;18:301.
[25] Li YJ, Kuo SW, Huang WJ, Lee HY, Chang FC. J Polym Sci, Part B: Polym Phys 2004;42:1127.
[26] Lichtenhan JD, Haddad TS, Schwab JJ, Carr MJ, Chaffee KP, Mather PT. Polym Prepr 1998;39:489.
[27] Waddon AJ, Coughlin EB. Chem Mater 2003;15:4555.